



Binary mixtures of bent-core molecules forming distinct types of B4 phase nano- and microfilament morphologies

Jiao Liu^a, Sasan Shadpour^a, Ahlam Nemati^a, Marianne E. Prévôt^a, Elda Hegmann^{a,b,c}, Chenhui Zhu^d and Torsten Hegmann^{a,b,e}

^aMaterials Science Graduate Program, Advanced Materials and Liquid Crystal Institute, Kent State University, Kent, OH, USA; ^bBrain Health Research Institute, Kent State University, Kent, OH, USA; ^cDepartment of Biological Sciences, Kent State University, Kent, OH, USA; ^dAdvanced Light Source, Lawrence Berkeley National Laboratory, Berkeley, CA, USA; ^eDepartment of Chemistry and Biochemistry, Kent State University, Kent, OH, USA

ABSTRACT

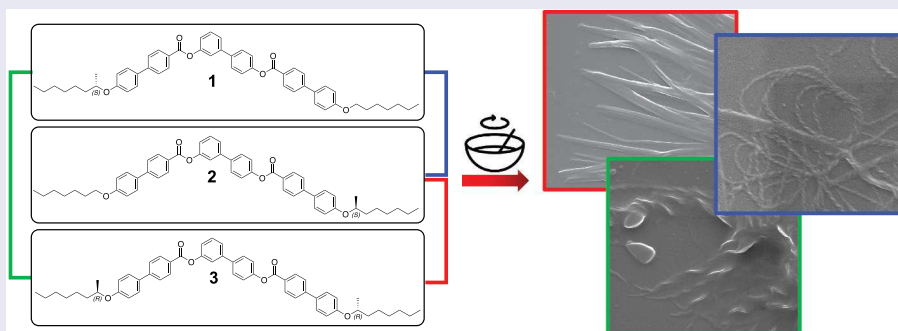
The remarkable ability of certain molecules with a bent molecular shape to form hierarchically self-assembled helical building blocks with negative Gaussian or cylindrical curvature featuring in-layer hexatic ordering—so-called B4 phases—has quickly transformed these molecules into desirable building blocks for a variety of potential applications in optics, energy harvesting, and metamaterials. We here demonstrate that these building blocks, helical nanofilaments, helical microfilaments, and heliconical-layered nanocylinders, can to some degree be predictably blended. Supported by scanning as well as transmission electron microscopy and variable angle x-ray scattering data, the three bent-core compounds, each forming exactly one of these B4 morphologies, in binary mixtures at a 1:1 molar ratio, form either the third missing, or one of the two but with opposite handedness, or a random mixture of the two selected morphologies with larger overall dimensions. Furthermore, for two of the mixtures the a priori predicted handedness of the chiral filaments was experimentally confirmed. The third mixture with a priori predicted antagonistic handedness of the initial morphologies forms a combination of the two, one apparently achiral and the other one with opposite handedness.

ARTICLE HISTORY

Received 19 October 2020
Accepted 3 November 2020

KEYWORDS



Bent-core liquid crystals; helical nanofilaments; chirality; helical microfilaments; binary mixtures



1. Introduction

Polymorphism, the ability of certain compounds that are chemically identical to exist in more than one form that differs in physical properties such as density, crystal structure, spectral signatures, melting point, or solubility [1], is of major concern in drug and materials development [2]. Similarly, polymorphism of chemical elements, termed allotropy, has equally impactful consequences in many branches of chemistry and materials science. For example, in the case of carbon, its allotropy encompasses distinct polymorphic shapes such as

fullerenes, nanotubes, carbon nanofoams, and graphene sheets in addition to graphite, diamond, lonsdaleite, as well as amorphous carbon among others [3]. Here, differences in structure determine shape and greatly impact macroscopic properties. A prime example of polymorphism in soft matter is the liquid crystalline state, where multiple forms (phases) can be observed for a given material depending on temperature or the concentration of an amphiphilic species such as surfactants, anisometric clays and nanomaterials, aggregates of molecules, etc., in a solvent, and further affected by

CONTACT Torsten Hegmann  thegmann@kent.edu
 Supplemental data for this article can be accessed [here](#).

© 2020 Informa UK Limited, trading as Taylor & Francis Group

temperature [4–8]. The self-assembly and degree of ordering (in one, two or three dimensions) in these phases can differ greatly, and a subset of these phases is characterised by the self-organisation of molecules and ensuing assemblies into distinct three-dimensional (3D) crystal lattices as in the case of blue phases [9–12] or by the self-organisation of the resulting quasi-crystalline building blocks. Among these phases, the so-called B4 phase formed by bent-core liquid crystals (BCLCs) stands out as a particularly intriguing example of morphological variety [13]. The B4 phase, while limited to certain subsets of bent-core molecules with specific molecular building blocks, results from the hierarchical self-assembly of twisted layer (tape) or helical ribbon morphologies at the nano- to mesoscale [14].

The classic description of the B4 phase was that of a crystalline solid [15]. However, the B4 phase based on the then discovered twisted tape morphology, also termed helical nanofilament (HNF) phase, forms due to an intralayer mismatch between the two molecular halves of the BCLC molecules that can only be relieved by local saddle splay. This ultimately leads to twisted filaments composed of a limited number of layer stacks (~5–7 layers) [13,16]. In the case of achiral BCLC molecules, HNFs form conglomerates composed of equal portions of macroscopic chiral domains with filaments of opposite handedness [17]. Ultimately, the B4 phase is neither a traditional crystalline solid nor a conventional liquid crystal phase [18]. The internal structure of these porous filaments shows hexatic liquid crystal ordering [13,17] but the overall, structure is predominantly crystalline as determined by solid-state NMR [18].

For a specific class of BCLCs with tris-biphenyl diester (tris-BiPh) central bent-core, subtle modifications of the molecular structure led to the discovery of a modulated HNF phase (HNF_{mod}) [14] featuring an additional intralayer electron-density modulation, two types of dual modulated HNF phases (HNF_{mod2a} and HNF_{mod2b}) [19,20] with additional intra- as well as interlayer modulations, but differing in inner symmetry and dimensions, by introducing chiral centres to both aliphatic chains with either identical or opposite absolute configuration. In due course, a theretofore never observed type of polymorphism was discovered for these tris-BiPh BCLCs when a single chiral centre was exclusively introduced at the shorter *meta*-side of these molecules [21]. In this case, the formation of entirely different phase structures was described solely depending on the rate of cooling from the isotropic liquid phase. Upon rapid cooling at a rate of $\geq 50^\circ\text{C min}^{-1}$, a B4 phase with another morphology was detected, best described as helical microfilaments (H μ Fs) based on the much larger dimensions of the stacked twisted tape

building blocks. Astoundingly, upon slow cooling at a rate of 5°C min^{-1} an oblique columnar (Col_{ob} – B1-type) LC phase was formed by these materials [21]. By moving the chiral centre to the other side chain, the longer *para*-side of the molecule, yet another morphology was uncovered. Unlike the molecules of this series described thus far, in the bulk these derivatives formed heliconical-layered nanocylinders (HLNCs) – coaxial layers of helical ribbons – composed of up to ten coaxial heliconical layers with cylindrical curvature. These HLNCs can split or merge, braid, and self-assemble into a variety of 3D superstructures including feather-like, herringbone, concentric rings, or hollow nest structures, largely controlled by adjusting the sample thicknesses and selecting appropriate substrates [22]. Similar morphologies such as helical ribbons, nanotubes, and twisted fibres have been reported by others including for BCLCs in binary mixtures with rod-like nematic LCs [23] or for ionic BCLC amphiphiles in water [24].

Considering that all four distinct B4-phase morphologies are formed by constitutional isomers, whereby chiral centres were strategically introduced at one (either the shorter *meta*- or the longer *para*-side) or both aliphatic side chains, we here explored possible binary blends between three derivatives of this series forming HNF_{mod2a}, H μ F and HLNC morphologies, respectively, at a 1:1 molar ratio. The notion of a blend here refers to the mixing of two solids with the product of the blending process showing properties unlike the sum of the individual components [25]. The resulting 1:1 mixtures were then analysed by cross-polarised light optical microscopy (POM), scanning as well as transmission electron microscopy (SEM, TEM), and x-ray scattering (XRS).

2. Results and discussion

The three B4 materials studied in these blending experiments, *meta*-(S)-1, *para*-(S)-2, and (*R,R*)-3, their distinct structural colour, morphology, and their phase sequences as well as phase transition temperatures depending on the cooling rate from the isotropic liquid phase are summarised in Figure 1. Each compound forms exactly one of the three B4 morphologies, HNF_{mod2a}, H μ F, and HLNC, and in sum all chiral centres present in the system would lead to a racemic ternary mixture. (*R,R*)-3 forms the B4 phase with HNF_{mod2} morphology independent of the cooling rate, *meta*-(S)-1 as well as *para*-(S)-2 show polymorphism depending on the cooling rate; between the B1 and B4 phase for *meta*-(S)-1 and distinguished by the space group (symmetry) of the B1 phases for *para*-(S)-2. In addition, *para*-(S)-2 shows some biphasic behaviour upon rapid cooling as

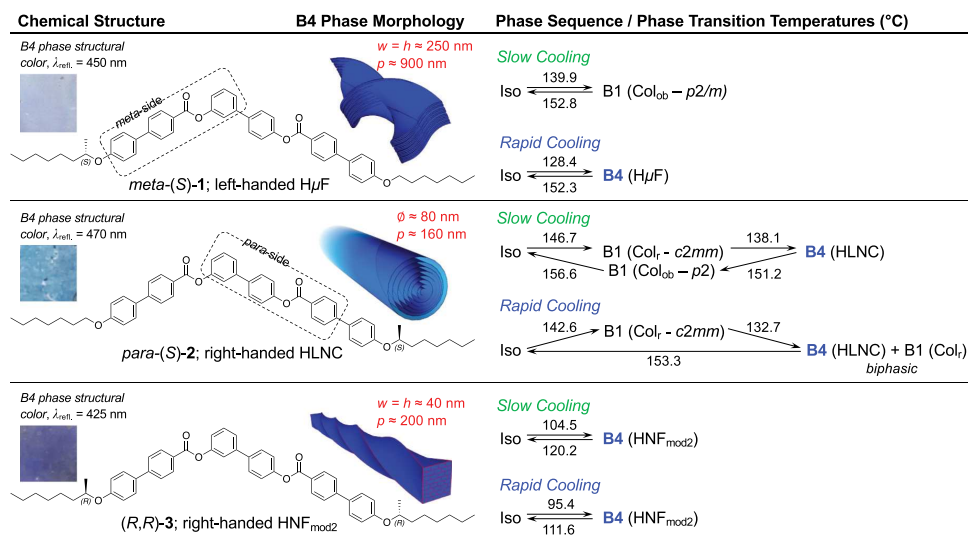


Figure 1. (Colour online) Chemical structures of the three B4 materials, *meta*-(S)-1 [21], *para*-(S)-2 [22], and (R,R)-3 [20], photograph of their distinct structural colours, B4-phase morphologies, and phase sequences as well as phase transition temperatures in °C depending on the cooling rate from the isotropic liquid phase. Slow cooling: 5°C min⁻¹, rapid cooling: $\geq 50^\circ\text{C min}^{-1}$.

determined earlier by small-angle X-ray scattering [22]. In light of this phase behaviour, the three binary mixtures were examined after rapid cooling from the isotropic liquid phase at a rate of $\geq 50^\circ\text{C min}^{-1}$ to ascertain the morphology by SEM and TEM, and at either cooling rate to examine miscibility and study texture evolution using both contact preparations and blends by POM.

2.1. POM, SEM and TEM characterisation

The first binary blend, a 1:1 mixture of *meta*-(S)-1 and *para*-(S)-2, yields [*meta*-(S), *para*-(S)-1/2] – a combination that would result in a theoretical net or sum compound (as indicated by the square brackets) featuring a chiral centre with (S)-configuration in each of the two chiral side chains, which is *de facto* identical to the homochiral (R,R)-3 analogue, *i.e.* (S,S)-3 [21], with opposite configuration of each chiral centre. (S,S)-3, as (R,R)-3, forms only the B4 phase at any given cooling rate from the isotropic liquid phase and is comprised of left-handed HNF_{mod2a} building blocks exhibiting an additional left-handed secondary twist among filaments in the bulk [20]. Blending the H μ F morphology of *meta*-(S)-1 with the HLNC morphology of *para*-(S)-2 should *a priori* give rise to a left-handed and blending of *meta*-(S)-1 with (R,R)-3 to a right-handed morphology based on the combination of chiral centres involved in each blend and their position in the *meta*- or *para*-side of the hypothetical molecule realised with the 1:1 blend (Figure 2(a)) [19].

For [*meta*-(rac), *para*-(R)-1/3], one combination of the two chiral centres mimics (R,R)-3, which forms a right-handed HNF_{mod2a}, and the other combination, *meta*-(S)- and *para*-(R), a right-handed HNF_{mod2b} morphology (Figure 2(b)). With respect to the latter combination of chiral centres, experimental SEM and TEM imaging data supported by density functional theory calculations and stochastic dynamic atomistic simulations confirmed that the configuration of the chiral centre in the longer *para*-side of these molecules determines the handedness of the HNF_{mod2} morphologies in these B4 phases ((S)- leading to left-handed and (R)- leading to right-handed HNF_{mod2(a/b)}) [19]. A conflict of handedness arises for the blend of *para*-(S)-2 with (R,R)-3 ([*meta*-(R), *para*-(rac)-2/3]). While each individual compound forms a right-handed B4 morphology, analysis of the configurations of the involved chiral centres reveals, based on the afore-mentioned calculations and imaging data [19], that combinations of the involved configuration of the chiral centres would lead to the opposite handedness of the blended B4-morphology. Hence, one might expect that the ensuing B4-morphology would not show signs of shape chirality such as a discernable handedness or maybe that such mismatch could lead to some sort of phase or morphology separation (Figure 2(c)).

Experimentally, prior to examining the blends by SEM, TEM and XRS, contact preparations between the relevant materials were prepared and studied by POM to examine the extent of miscibility and thereby the phase behaviour in the contact zone between the two components constituting each blend.

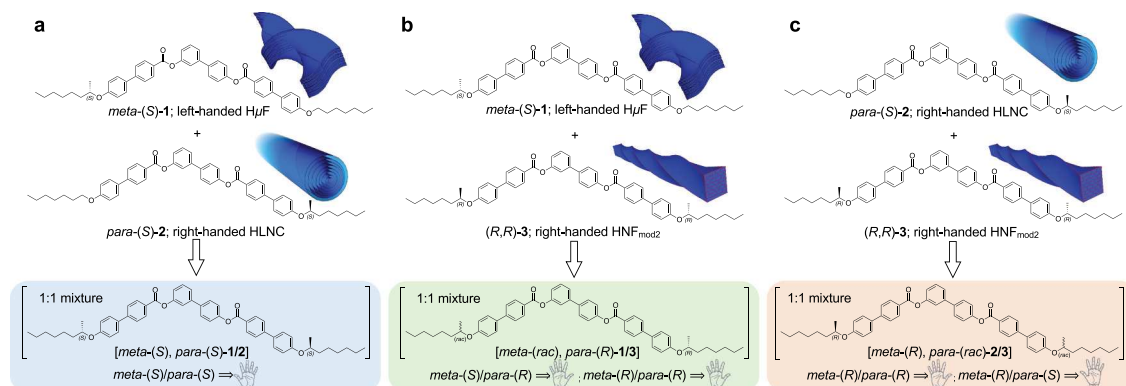


Figure 2. (Colour online) Chemical structures and B4-phase morphologies of the BCLCs studied in 1:1 blends: (a) [*meta*-(S), *para*-(S)-1/2], (b) [*meta*-(rac), *para*-(R)-1/3], and (c) [*meta*-(R), *para*-(rac)-2/3] each with an *a priori* analysis of the anticipated handedness of the B4 morphologies.

For [*meta*-(S), *para*-(S)-1/2], the two individual compounds, *meta*-(S)-1 and *para*-(S)-2, show no miscibility irrespective of the cooling rate, *i.e.* between the Col_{ob} phase of *meta*-(S)-1 and the HLNC morphology of *para*-(S)-2 on slow cooling as well as the HμF and HLNC morphologies of the two B4 phases upon rapid cooling (Figure 3(a,b)). POM images of the 1:1 blend, however, show textures typically observed for HNF_{mod} B4 phases (Figure 3(c,d), as well as Figure S1 (Supplementary Data) that shows photomicrographs of a temperature scan on cooling) with no indication of adjacent domains with opposite chirality (or handedness) upon decrossing the polarisers [19,20].

SEM as well as TEM then confirm the formation of HNFs with dimensions of about 100 nm in width (*w*) and a helical pitch (*p*) of about 400 nm; closely matching the dimensions of the recently discovered larger HNF_{mod2b} for the compounds with opposite configuration of the chiral centres in each side chain [19] (Figure 4 and Figure S2, Supplementary Data). As anticipated *a priori*, the handedness of the resulting HNFs is left-handed just as for the HNF_{mod2a} morphology formed by (S,S)-3 reported earlier [20]. Most notably, blending of HμF and HLNC B4 morphologies in essence gives rise to the HNF_{mod2b} morphology with overall dimensions for *w* and *p* roughly between the two original HμF and HLNC morphologies. In addition,

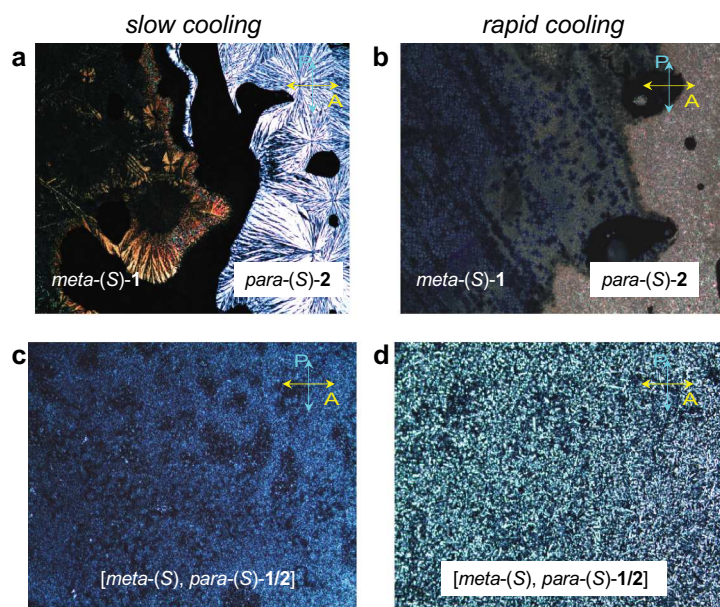


Figure 3. (Colour online) POM photomicrographs (crossed polarisers) taken at room temperature (20°C) for the 1:1 blend of *meta*-(S)-1 and *para*-(S)-2 ([*meta*-(S), *para*-(S)-1/2]): (a, b) contact preparations observed (a) upon slow cooling and (b) upon rapid cooling; (c, d) 1:1 blend observed (c) upon slow cooling and (d) upon rapid cooling.

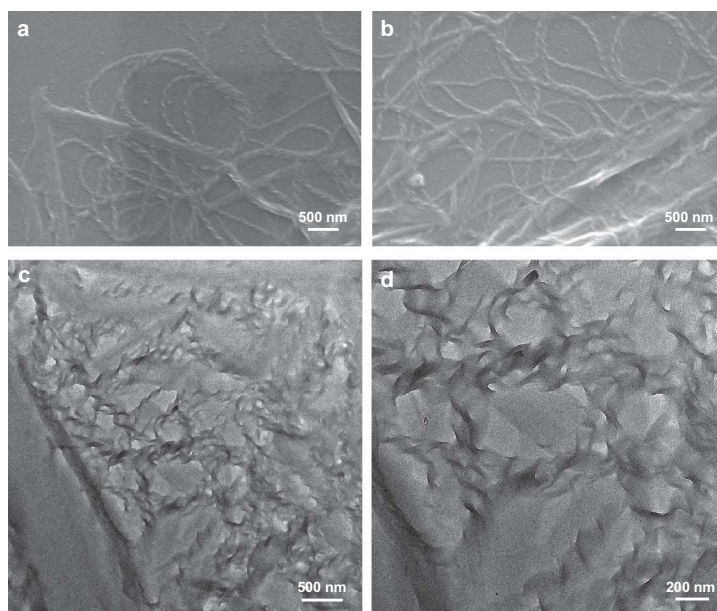


Figure 4. Electron microscopy images of the 1:1 blend of *meta*-(*S*)-**1** and *para*-(*S*)-**2** ([*meta*-(*S*), *para*-(*S*)-**1/2**]): (a, b) SEM and (c, d) TEM. Note that exclusively left-handed HNFs are formed.

however, some of the SEM and TEM images additionally show a nanocylinder morphology, thereby indicating a certain degree of coexistence with the HNFs, which clearly appear to be in the majority. In certain cases, the HNFs almost seem to adorn the cylinders, mimicking the appearance of the bird's nest fern leaves (Figures S2d – S2f; see Supplemental Data).

For [*meta*-(*rac*), *para*-(*R*)-**1/3**], POM images of the contact preparation between *meta*-(*S*)-**1** and (*R,R*)-**3**

show a significant degree of miscibility upon slow cooling, whereby the grainy texture of *meta*-(*S*)-**1** with low birefringence meets the even less birefringent dark texture formed by (*R,R*)-**3**. This contact region is characterised by a feather-like texture, which exhibits the highest birefringence (Figure 5(a)). Upon rapid cooling, this contact zone shows the appearance of a bright blue band (centre of the image), again characterised by the highest birefringence (Figure 5(b)). We note that the comparatively low

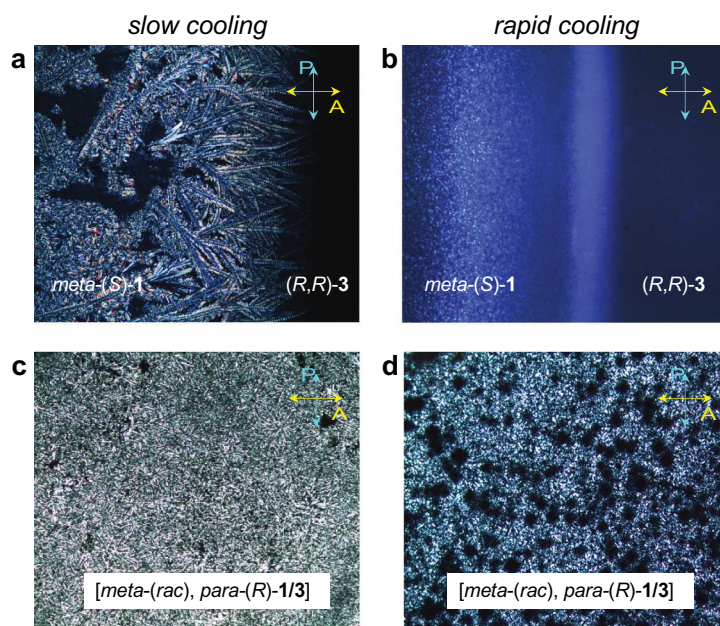


Figure 5. (Colour online) POM photomicrographs (crossed polarisers) taken at room temperature (20°C) for the 1:1 blend of *meta*-(*S*)-**1** and (*R,R*)-**3** ([*meta*-(*rac*), *para*-(*R*)-**1/3**]): (a, b) contact preparations observed (a) upon slow cooling and (b) upon rapid cooling; (c, d) 1:1 blend observed (c) upon slow cooling and (d) upon rapid cooling.

birefringence texture formed by (R,R) -**3** is here more visible than in the POM image taken at a slow cooling rate. These contact preparations suggest that a new morphology might be expected for the blend. However, POM images taken for the 1:1 blend show a texture (Figure 5(c,d), as well as Figure S3 (Supplementary Data) showing

micrographs of a temperature scan on cooling) closely resembling those for $[meta-(S), para-(S)-1/2]$ (Figure 3 (c,d)).

SEM as well as TEM imaging reveal a type of filament with a large helix angle [26] and dimensions of about 200–300 nm in width and 500 to almost 900 nm for the

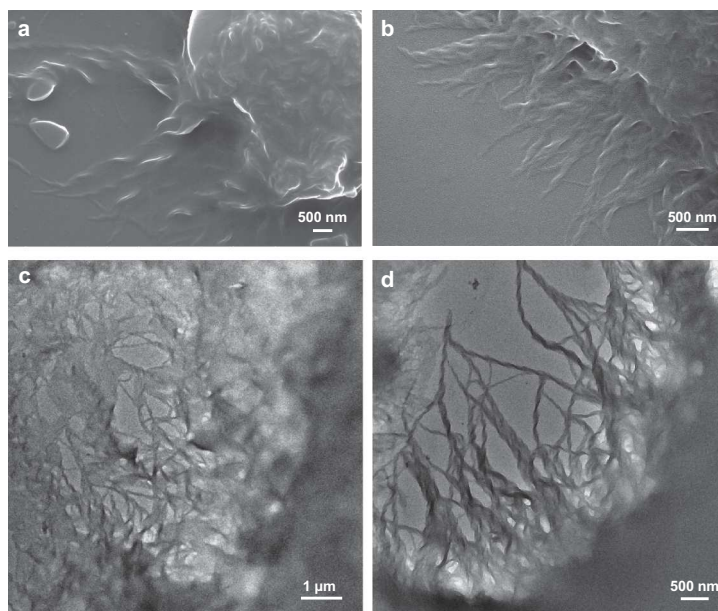


Figure 6. Electron microscopy images of the 1:1 blend of $meta-(S)$ -**1** and (R,R) -**3** ($[meta-(rac), para-(R)-1/3]$): (a, b) SEM and (c, d) TEM. Note that exclusively right-handed H μ Fs are formed.

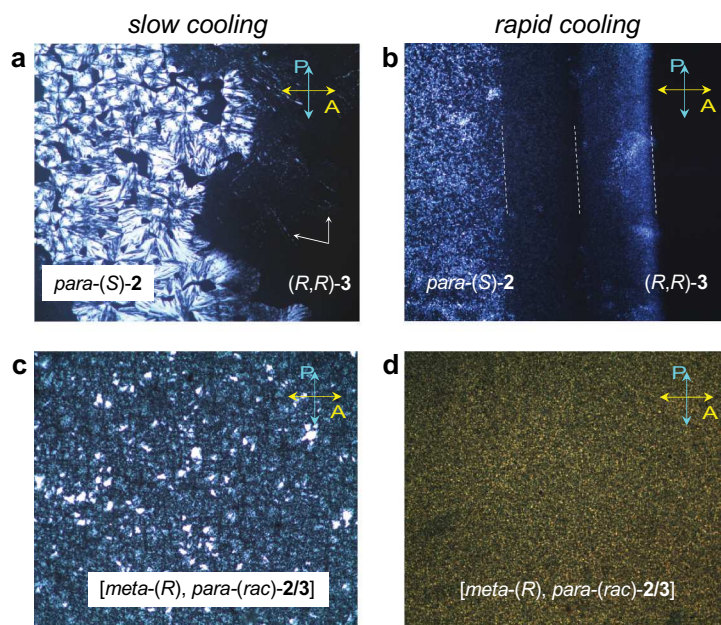


Figure 7. (Colour online) POM photomicrographs (crossed polarisers) taken at room temperature (20°C) for the 1:1 blend of $para-(S)$ -**2** and (R,R) -**3** ($[meta-(R), para-(rac)-2/3]$): (a, b) contact preparations observed (a) upon slow cooling (white arrows point at the birefringent threads) and (b) upon rapid cooling (white dashed lines emphasise the two new phases or morphologies); (c, d) 1:1 blend observed (c) upon slow cooling and (d) upon rapid cooling.

helical pitch more closely resembling those of the H μ F morphology (see Figure 6 as well as Figure S4, Supplementary Data) [21]. The *a priori* predicted handedness (right-handed) is also preserved throughout all SEM and TEM images similar to the H μ Fs formed by *meta*-(*R*)-1 exclusively upon rapid cooling [21]. In this particular case, the conformation of the chiral centre in the longer *para*-side again dictates the handedness (assuming the experimental data from the homo- and heterochiral HNF_{mod2(a,b)} morphologies) [19], and the presence of a chiral centre in the shorter *meta*-side the overall morphology. Contrary to [*meta*-(*S*), *para*-(*S*)-1/2], [*meta*-(*rac*), *para*-(*R*)-1/3], formed by mixing compounds forming B4 phases with H μ F and HNF_{mod2a} morphologies, does not form the third and missing morphology (here HLNC), but forms filaments with dimensions similar to the H μ Fs.

For the final binary blend [*meta*-(*R*), *para*-(*rac*)-2/3], POM images of contact preparations between *para*-(*S*)-2 and (*R,R*)-3 again show one additional texture (phase) upon slow cooling (Figure 7(a)) and even two upon rapid cooling (Figure 7(b)). On slow cooling, the contact zone studied by POM displays thin birefringent threads (similar to dashed lines; indicated by white arrows in Figure 7(a)) and on rapid cooling two distinct blue bands with lower birefringence than *para*-(*S*)-2 at centre left, but higher birefringence than (*R,R*)-3 at the centre right of the photomicrograph (indicated by two white, dashed lines in Figure 7(b)). With the electron microscopy studies all performed with samples prepared

using rapid cooling, this observation perhaps forebodes the formation of two added morphologies. POM investigations of this blend ([*meta*-(*R*), *para*-(*rac*)-2/3]) show textures (Figure 7(c,d), as well as Figure S5 (Supplementary Data) showing micrographs of a temperature scan on cooling) that bear resemblance to those for neat *para*-(*S*)- and *para*-(*R*)-2 reported previously; blueish focal-conic like domains upon slow cooling (not especially well-defined) and a grainy texture similar to the B1-domains of the biphasic system obtained upon rapid cooling [22]. Such phase behaviour could suggest that [*meta*-(*R*), *para*-(*rac*)-2/3] forms a B4 phase with HLNC morphology just as *para*-(*S*)-2. The configuration of all involved chiral centres and again assuming *a priori* that the handedness imposed by the longer *para*-side of the net or sum molecule [*meta*-(*R*), *para*-(*rac*)-2/3] would suggest that the resulting filaments would not display any preferred handedness.

SEM and TEM imaging, however, show a coexistence of two morphologies, one resembling HLNCs and a left-handed HNF morphology (see Figure 8 as well as Figure S6, Supplementary Data). This is particularly evident in the SEM image in Figure 8(b) (lower and upper left-hand corner of the image) and in the two TEM images shown in Figure 8(c,d). The nanocylinder-like morphology is characterised by smooth, often pointy features varying in diameter (these could perhaps also be nanotubules, although TEM images show no contrast variation across these filaments, thus supporting a nanocylinder morphology) without any visual evidence

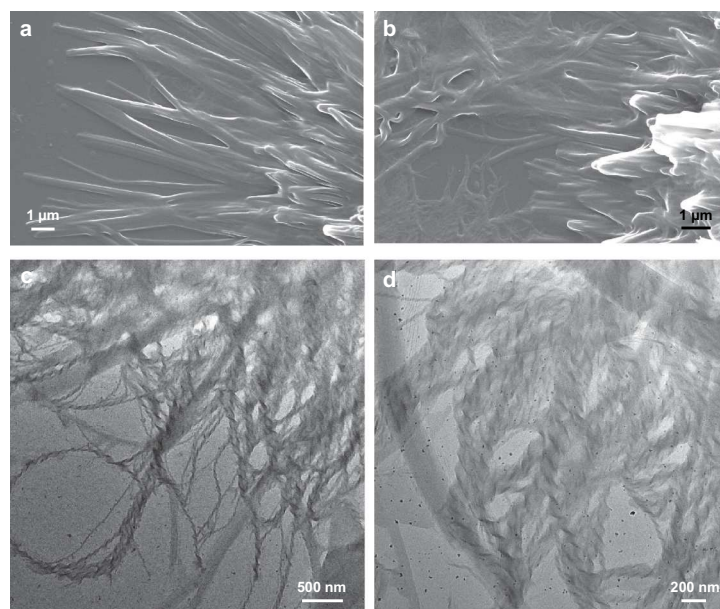


Figure 8. Electron microscopy images of the 1:1 blend of *para*-(*S*)-2 and (*R,R*)-3 ([*meta*-(*R*), *para*-(*rac*)-2/3]): (a, b) SEM and (c, d) TEM. Note that exclusively left-handed HNFs are formed simultaneously with smooth cylinder-like filaments.

of heliconical layering (or layering of helical ribbons) frequently bundling together with a diameter ranging from about 200–600 nm (most average about 350 nm).

The simultaneously observed HNFs are on average 70 nm in width with an average helical pitch of about 200 nm and are all exclusively left-handed. These filament dimensions are most similar to those of the classical HNF [13], HNF_{mod} [14] or HNF_{mod2a} [20] morphologies, but their left-handedness (visible only in the TEM images) is puzzling considering that the HNF component in this particular blend, *i.e.* (R,R)-3, forms a B4 phase with exclusively right-handed HNF_{mod2a} twisted layer filaments. Only one of the two combinations of the involved chiral centre configurations (*meta*-(R)/*para*-(S), see Figure 2) supports this handedness of the HNFs if, as in all other cases, the configuration of the chiral centre in the longer *para*-side determines filament handedness.

Another question arises from the fact that only this particular mixture shows coexistence of two morphologies. POM studies of contact preparations between *para*-(S)-2 and (R,R)-3 (Figure 7(b)) already implied this by showing two additional phases or morphologies in the contact zone. All current and previous POM studies of contact preparations [20,21] revealed that the various B4 morphologies do not mix because shapes are incommensurate or the handedness is opposite, frequently accompanied by the induction of additional phases. In contact preparations the two components are forced into contact as melts (isotropic liquids); here all mixtures investigated by electron microscopy of POM (as blends) were mixed using an organic solvent prior to heating into the isotropic liquid phase and subsequent rapid cooling to room temperature. Nevertheless, the mixture between *para*-(S)-2 and (R,R)-3 is the one with the largest difference in phase transition temperatures from the isotropic liquid to the B1 or B4 phase upon rapid cooling ($\Delta T_{\text{Iso-B}} = 47.2^\circ\text{C}$). The blends [*meta*-(S), *para*-(S)-1/2] and [*meta*-(rac), *para*-(R)-1/3] show notably lower differences in this phase transition temperature; $\Delta T_{\text{Iso-B}} = 14.2^\circ\text{C}$ and $\Delta T_{\text{Iso-B}} = 33.0^\circ\text{C}$, respectively. If such difference in phase transition temperatures upon rapid cooling drives the simultaneous formation of two B4 morphologies it would imply some degree of self-sorting – molecules that form HLNCs and molecules that form HNFs. The two observed morphologies are, however, unlike the two morphologies being mixed initially. The nanocylinders are much larger with respect to their average diameter and smooth showing no features in the electron microscopy images of any heliconical layering; the HNFs are just slightly larger in width and height, identical in helical pitch, but have opposite handedness. One possible explanation could be that two fractions are being formed upon rapid cooling, one rich in *para*-(S)-2 and one rich in (R,R)-3. *Para*-(S)-2 could then serve as a chiral additive affecting the formation of larger HNFs with a given

handedness (an (S)-configuration of the chiral centre in these tris-biphenyl derivatives leads to left-handed HNFs), and (R,R)-3 would serve as additives, driving the formation racemic nanocylinders because the longer *para*-side of the molecules in the blend experiences a lower enantiomeric excess (no longer pure (S)- by adding some amount of (R)-configuration). Oddly, the blend [*meta*-(S), *para*-(S)-1/2] also showed coexistence of two morphologies despite the lowest $\Delta T_{\text{Iso-B}}$ of only 14.2°C . In this case, however, the additionally observed nanocylinders are just a minor component of a blend otherwise dominated by the formed HNF_{mod2b} morphology.

2.2. X-ray scattering studies

To unequivocally confirm phase assignment and structure of the B4 phases formed by the three binary mixtures we performed X-ray scattering experiments after heating the samples to the isotropic liquid phase (180°C) and subsequently cooling to room temperature (20°C) at a rate $\geq 50^\circ\text{C min}^{-1}$ in the *q*-range (momentum transfer range) from 0.1 to 1.7 \AA^{-1} . The diffraction patterns shown in Figure 9 clearly indicate that all three blends are layer structures like all other B4 phase morphologies as well as the typical noncommensurate high-*q* maxima signifying the commonly observed crystalline nature of the B4 phase (Figure 9). A comparison of the current to the X-ray scattering patterns previously obtained for the various B4 morphologies reveals that the pattern obtained for [*meta*-(S), *para*-(S)-1/2] (Figure 9; blue curves) closely matches the pattern obtained for (R,R)-3 (or (S,S)-3) forming a B4 phase with HNF_{mod2a} morphology [20], but also suggests additional features from the XRS pattern of the HLNCs [22]. Complicating the matter is that the peaks overlap, which corresponds to the varying internal structures of each filament type [20–22]. However, deconvolution of the low-*q* peaks (see Figure S7 and Table S1) then reveals what was already seen by SEM and TEM imaging, a coexistence of the HNF_{mod2} and another B4 phase nanocylinder morphology and superposition of the two separate XRS plots would provide the blue curve shown in Figure 9. Analogously, the scattering pattern acquired for [*meta*-(rac), *para*-(R)-1/3] (see Figure 9; green curves as well as Figure S8 and Table S2, Supplemental Data) largely coincides with the one obtained for *meta*-(S)-2 [21], even the maxima indicating the coexistence of the B4 H μ F phase with the B1 (Col_{ob}) phase [21]. In fact, several of the SEM and TEM images of [*meta*-(rac), *para*-(R)-1/3] show areas with less defined H μ Fs and additional wavy bulk structures (see Figure 6(a,b) as well as Figures S4a and S4c) like those recorded previously by SEM for the B1 (Col_{ob}) phase formed by *meta*-(S)-2 [21]. Finally, the pattern for [*meta*-(R), *para*-(rac)-2/3] appears most similar to an average of the patterns previously obtained for *para*-(S)-2 [22] and (R,R)-3 [20] (with respect to peak position and relative intensity),

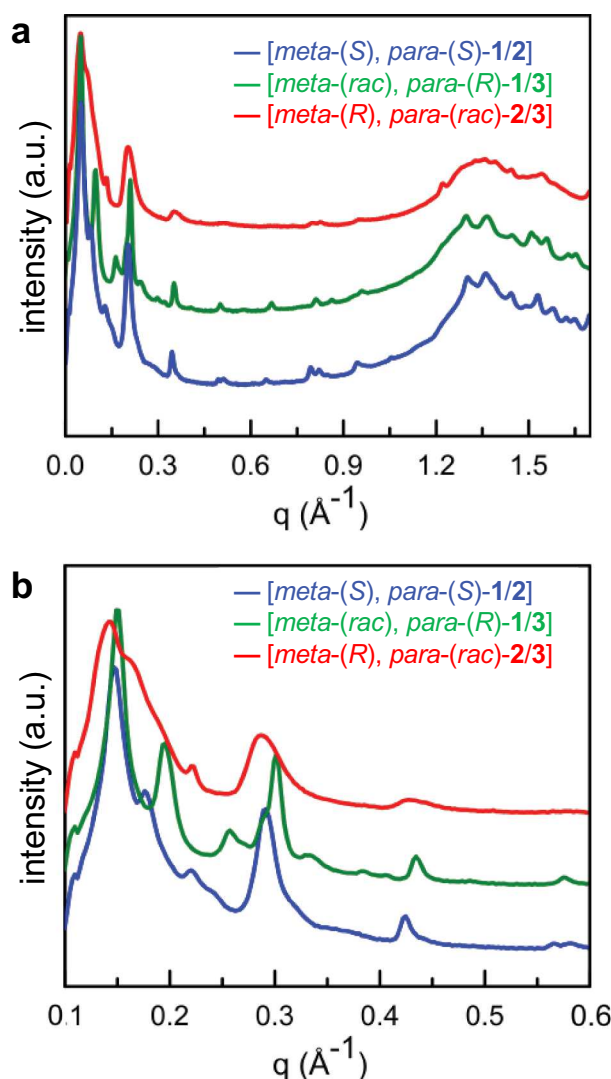


Figure 9. (Colour online) X-ray scattering analysis (azimuthally integrated intensity (a.u.) versus q (\AA^{-1}) after heating to the isotropic liquid phase followed by cooling to 20°C at $\geq 50^\circ\text{C min}^{-1}$: (a) comparison plot $0 \leq q \leq 1.7$ (\AA^{-1}) and (b) low q -range; $0.1 \leq q \leq 0.6$ (\AA^{-1}); $[meta-(S), para-(S)-1/2]$ – blue pattern, $[meta-(rac), para-(R)-1/3]$ – green pattern, and $[meta-(R), para-(rac)-2/3]$ – red pattern. Data with exact values for q , relative intensities, and indexing mapping the origin of the scattering maxima to the actual B4 morphology are provided in the Supplementary Data (Figures S7 – S9 and Tables S1 – S3).

which is conceivably also responsible for the peak broadening (larger FWHM) in comparison to the narrower peak widths seen for the other two blends (Figure 9; red scattering curve as well as Figure S9 and Table S3). As such, the collected XRS data fully support both the SEM and the TEM imaging results, which showed clear coexistence of some form of nanocylinders and HNFs.

3. Conclusions

In conclusion, we establish that B4-phase morphologies such as HNF_{mod2} , $\text{H}\mu\text{F}$, and HLNC can be mixed using an organic solvent leading to three distinct blends that exhibit quasi the entire range of B4 morphologies with varying degree of coexistence, with similar or entirely new

dimensions with respect to height, width, diameter, and helical pitch. The data continue to support theoretical as well as experimental data that the configuration of the chiral centre in the aliphatic chain attached to the longer *para*-side dictates the handedness of the resulting filaments. *A priori* predictions of the filaments' handedness by considering the configurations of the chiral centres involved are confirmed experimentally. This includes the observed racemic nature of the nanocylinders, where the side chain of the sum or net compound is racemic in the *para*-side. Because of this, the observed nanostructures lack signs of helical layering. A similar, but thermoreversible process has been observed for peptide amphiphiles, where helical ribbons or tubules can be reversibly switched to twisted tapes [27,28]. Finally, XRS analyses of

the blends at room temperature support the results obtained by electron microscopy, and even captures the coexistence of two simultaneously formed morphologies or phases in each of these three blends. Thus, one could argue that these, particularly in the cases of [*meta*-(S), *para*-(S)-1/2] and [*meta*-(rac), *para*-(R)-1/3], are cases of a coexistence of cocrystals, where one or more components form unique crystalline solids that here coexist in the form of the various filaments as defined by Stahly [29]. However, in the case of [*meta*-(R), *para*-(rac)-2/3], the two original filament types coexist but appear to be doped by one another affecting the resulting handedness or lack thereof. Overall, these data demonstrate that complex nano- or microscale morphologies can be blended with fairly predictable outcomes *vis-à-vis* shape and especially filament handedness, which could further support various applications of these fascinating materials and morphologies for structural colour reflectors, chiral detection, and photonic films for security applications among others as recently demonstrated by Yoon and co-workers [30–33].

4. Experimental section

The synthesis of *meta*-(S)-1 (4'-[4-(4'-octyloxy)biphenyloxy]-3-[4-(4'-[2-(S)-heptan-2-yloxy]biphenyl)]-biphenyl), *para*-(S)-2 (4'-[4-(2-(S)-heptan-2-yloxy)biphenyloxy]-3-[4-(4'-[4'-octyloxy]biphenyl)] biphenyl), and (R,R)-3 (biphenyl-3,4'-diyl bis-(4'-[2-(R)-heptan-2-yloxy]biphenyl-4-carboxylate)) and the complete characterisation of these materials were reported previously [20–22]. Unless otherwise stated, all organic solvents used for the synthesis were EMD Millipore grade and purified by a PureSolv solvent purification system (Innovative Technology Inc.). Blends were prepared using standardised solutions of each compound in an organic solvent such as methylene chloride followed by mixing equal volumes of these solutions to produce each 1:1 mixture. Contact cells were prepared between two untreated microscope glass slides by filling the space between them using capillary forces starting with the compound with higher clearing point (*i.e.* the B1- or B4-phase to isotropic liquid phase transition temperature) followed by the one with lower clearing point until contact between the two components is established. POM observations were carried out using an Olympus BX-53 polarising microscope equipped with a Linkam LTS420E heating/cooling stage. SEM analysis was performed using a Quanta 450 FEG SEM on the direct sample without prior metal deposition. TEM was carried out on an FEI Tecnai F20 microscope, operating at 200 kV and equipped with a Schottky field emission gun and a twin-blade

anticontaminator. All images were recorded using a Gatan 4 K Ultra Scan charge-coupled device camera. As these organic material films are sensitive to the electron beam irradiation, the films were normally previewed rapidly at a dose of 20 e[−] nm^{−2}. Selected areas were then imaged at a dose level of 200 e[−] nm^{−2}, which we found did not cause any radiation damage. XRS was carried out on beamline 7.3.3 of the Advanced Light Source of Lawrence Berkeley National Laboratory [34] (10 keV incident beam energy, 1.24 Å wavelength, utilising a Pilatus 2 M detector). Prior to XRS analysis, materials were filled into 1 mm diameter quartz X-ray capillary tubes. The analysis was made in Igor Pro software with Nika package [35].

Acknowledgments

This work was supported by the U.S. National Science Foundation (NSF, DMR-1506018 and DMR-1904091), the Ohio Third Frontier (OTF) program for Ohio Research Scholars “Research Cluster on Surfaces in Advanced Materials” (T.H.), which also supports the Liquid Crystal Characterization facility at the Advanced Materials and Liquid Crystal Institute at Kent State University, where current SEM and TEM data were acquired. The authors are also grateful for access to the SAXS beamline at the Advanced Light Source, which is supported by the Director (Office of Science, Office of Basic Energy Sciences) of the U.S. Department of Energy under Contract No. DE-AC02-05CH11231.

Disclosure statement

There are no conflicts to declare.

ORCID

Elda Hegmann  <http://orcid.org/0000-0003-3287-5103>

Author contributions

T.H. and J.L. conceived the described experiment. S.S., A.N., and J.L. performed the syntheses and complete characterization of the materials. J.L. did the POM and SEM studies; A. N. performed the TEM experiments, and C.Z. the XRS studies. M.E.P., E.H. and T.H. analyzed the XRS data. T. H. directed the research and wrote the manuscript with contributions from all coauthors.

Funding

This work was supported by the Basic Energy Sciences [DE-AC02-05CH11231]; Division of Materials Research [1506018,1904091]; Ohio Third Frontier.

References

- [1] Cruz-Cabeza AJ, Reutzel-Edens SM, Bernstein J. Facts and fictions about polymorphism. *Chem Soc Rev*. 2015;44(23):8619–8635.
- [2] Datta S, Grant DJW. Crystal structures of drugs: advances in determination, prediction and engineering. *Nat Rev Drug Discov*. 2004;3(1):42–57.
- [3] Hirsch A. The era of carbon allotropes. *Nat Mater*. 2010;9(11):868–871.
- [4] Vorländer D. The polymorphism of liquid crystals. A - demonstration. *Trans Faraday Soc*. 1933;29:0913–0914.
- [5] Fehr C, Dieudonne P, Primera J, et al. Solid state polymorphism of liquid crystals in confined geometries. *Eur Phys J E*. 2003;12:S13–S16.
- [6] Prost J. Polymorphism and properties of liquid-crystals. *Chimia (Aarau)*. 1984;38(7–8):260–261.
- [7] Sackmann H. Thermodynamic aspects of polymorphism in liquid-crystals. *Pure Appl Chem*. 1974;38(4):505–527.
- [8] Sackmann H, Demus D. Problems of polymorphism in liquid-crystals. *Mol Cryst Liq Cryst*. 1973;21(3–4):239–273.
- [9] Coles HJ, Pivnenko MN. Liquid crystal ‘blue phases’ with a wide temperature range. *Nature*. 2005;436(7053):997–1000.
- [10] Oton E, Netter E, Nakano T, et al. Monodomain blue phase liquid crystal layers for phase modulation. *Sci Rep*. 2017;7:44575.
- [11] Kitzerow HS. Blue phases come of age: a review. *Proc SPIE*. 2009;7232:723205.
- [12] Salamończyk M, Vaupotic N, Pocięcha D, et al. Structure of nanoscale-pitch helical phases: blue phase and twist-bend nematic phase resolved by resonant soft X-ray scattering. *Soft Matter*. 2017;13(38):6694–6699.
- [13] Hough LE, Jung HT, Krueker D, et al. Helical nanofilament phases. *Science*. 2009;325(5939):456–460.
- [14] Tsai E, Richardson JM, Korblova E, et al. A modulated helical nanofilament phase. *Angew Chem Int Edit*. 2013;52(20):5254–5257.
- [15] Pelzl G, Diele S, Weissflog W. Banana-shaped compounds - A new field of liquid crystals. *Adv Mater*. 1999;11(9):707–724.
- [16] Zhu CH, Wang C, Young A, et al. Probing and controlling liquid crystal helical nanofilaments. *Nano Lett*. 2015;15(5):3420–3424.
- [17] Chen D, Tuchband MR, Horanyi B, et al. Diastereomeric liquid crystal domains at the mesoscale. *Nat Commun*. 2015;6:7763.
- [18] Walba DM, Eshdat L, Korblova E, et al. On the nature of the B4 banana phase: crystal or not a crystal? *Cryst Growth Des*. 2005;5(6):2091–2099.
- [19] Shadpour S, Nemati A, Salamończyk M, et al. Missing link between helical nano- and microfilaments in B4 phase bent-core liquid crystals, and deciphering which chiral center controls the filament handedness. *Small*. 2019;16(4):1905591.
- [20] Li L, Salamończyk M, Jákli A, et al. A dual modulated homochiral helical nanofilament phase with local columnar ordering formed by bent core liquid crystals: effects of molecular chirality. *Small*. 2016;12(29):3944–3955.
- [21] Li L, Salamończyk M, Shadpour S, et al. An unusual type of polymorphism in a liquid crystal. *Nat Commun*. 2018;9:714.
- [22] Shadpour S, Nemati A, Boyd NJ, et al. Heliconal-layered nanocylinders (HLNCs) - hierarchical self-assembly in a unique B4 phase liquid crystal morphology. *Mater Horiz*. 2019;6(5):959–968.
- [23] Gorecka E, Vaupotic N, Zep A, et al. From sponges to nanotubes: A change of nanocrystal morphology for acute-angle bent-core molecules. *Angew Chem Int Edit*. 2016;55(40):12238–12242.
- [24] Castillo-Valles M, Cano M, Bermejo-Sanz A, et al. Towards supramolecular nanostructured materials: control of the self-assembly of ionic bent-core amphiphiles. *J Mater Chem C*. 2020;8(6):1998–2007.
- [25] Maynard E. Fundamentals of bulk solids mixing and blending. *Chem Eng*. 2013;120(9):66–71.
- [26] Kim H, Lee S, Shin TJ, et al. Multistep hierarchical self-assembly of chiral nanopore arrays. *Proc Natl Acad Sci USA*. 2014;111(40):14342–14347.
- [27] Hamley IW, Dehsorkhi A, Castelletto V, et al. Reversible helical unwinding transition of a self-assembling peptide amphiphile. *Soft Matter*. 2013;9(39):9290–9293.
- [28] Dehsorkhi A, Castelletto V, Hamley IW. Self-assembling amphiphilic peptides. *J Pept Sci*. 2014;20(7):453–467.
- [29] Stahly GP. Diversity in single- and multiple-component crystals. The search for and prevalence of polymorphs and cocrystals. *Cryst Growth Des*. 2007;7(6):1007–1026.
- [30] Park W, Ha T, Kim TT, et al. Directed self-assembly of a helical nanofilament liquid crystal phase for use as structural color reflectors. *NPG Asia Mater*. 2019;11:45.
- [31] Park W, Wolska JM, Pocięcha D, et al. Direct visualization of optical activity in chiral substances using a helical nanofilament (B4) liquid crystal phase. *Adv Opt Mater*. 2019;7(23):1901399.
- [32] Park W, Yoon DK. Orientation control of helical nanofilament phase and its chiroptical applications. *Crystals*. 2020;10(8):675.
- [33] Park W, Ha T, Jung TS, et al. Security use of the chiral photonic film made of helical liquid crystal structures. *Nanoscale*. 2020. in press. DOI:10.1039/D0NR03743E.
- [34] Hexemer A, Bras W, Glossinger J, et al., XIV International Conference on Small-Angle Scattering (SAS09), Oxford (UK). 2010;247:012007.
- [35] Ilavsky J. Nika: software for two-dimensional data reduction. *J Appl Crystallogr*. 2012;45(2):324–328.